Published in final edited form as:
J Mol Cell Cardiol. 2009 June ; 46(6): 1027–1036. doi:10.1016/j.yjmcc.2009.03.015.

Mitochondrial Free Calcium Regulation during Sarcoplasmic Reticulum Calcium Release in Rat Cardiac Myocytes

Tatyana N. Andrienko, **Eckard Picht**, and **Donald M. Bers**
Department of Pharmacology, University of California Davis, Genome Building 3511, Davis, CA 95616-8636

Abstract

Cardiac mitochondria can take up Ca^{2+}, competing with Ca^{2+} transporters like the sarcoplasmic reticulum (SR) Ca^{2+}-ATPase. Rapid mitochondrial $[Ca^{2+}]$ transients have been reported to be synchronized with normal cytosolic $[Ca^{2+}]_i$ transients. However, most intra-mitochondrial free $[Ca^{2+}]$ ($[Ca^{2+}]_{mito}$) measurements have been uncalibrated, and potentially contaminated by non-mitochondrial signals. Here we measured calibrated $[Ca^{2+}]_{mito}$ in single rat myocytes using the ratiometric Ca^{2+} indicator fura-2 AM and plasmalemmal permeabilization by saponin (to eliminate cytosolic fura-2). The steady-state $[Ca^{2+}]_{mito}$ dependence on $[Ca^{2+}]_i$ (with 5 mM EGTA) was sigmoid with $[Ca^{2+}]_{mito} < [Ca^{2+}]_i$ for $[Ca^{2+}]_i$ below 475 nM. With low [EGTA] (50 μM) and 150 nM $[Ca^{2+}]_i$(±15 mM Na^+) cyclical spontaneous SR Ca^{2+} release occurred (5–15/min). Changes in $[Ca^{2+}]_{mito}$ during individual $[Ca^{2+}]_i$ transients were small (~2–10 nM/beat), but integrated gradually to steady-state. Inhibition SR Ca^{2+} handling by thapsigargin, 2 mM tetracaine or 10 mM caffeine all stopped the progressive rise in $[Ca^{2+}]_{mito}$ and spontaneous Ca^{2+} transients (confirming that SR Ca^{2+} releases caused the $[Ca^{2+}]_{mito}$ rise). Confocal imaging of local $[Ca^{2+}]_{mito}$ (using rhod-2) showed that $[Ca^{2+}]_{mito}$ rose rapidly with a delay after SR Ca^{2+} release (with amplitude up to 10 nM), but declined much more slowly than $[Ca^{2+}]_i$ (time constant 2.8 ±0.7 s vs. 0.19 ±0.06 s). Total Ca^{2+} uptake for larger $[Ca^{2+}]_{mito}$ transients was ~0.5 μmol/l cytosol (assuming 100:1 mitochondrial Ca^{2+} buffering), consistent with prior indirect estimates from $[Ca^{2+}]_i$ measurements, and corresponds to ~1% of the SR Ca^{2+} uptake during a normal Ca^{2+} transient. Thus small phasic $[Ca^{2+}]_{mito}$ transients and gradually integrating $[Ca^{2+}]_{mito}$ signals occur during repeating $[Ca^{2+}]_i$ transients.

Keywords

Mitochondria; calcium transport; cardiac myocytes; sarcoplasmic reticulum

Introduction

In cardiac myocytes, cytosolic Ca^{2+} concentration ($[Ca^{2+}]_i$) transiently increases during each heart beat, initiating cellular contraction, and decreases during diastole to allow relaxation. The majority of the energy needed for contraction and intracellular ion homeostasis is provided by mitochondria via oxidative phosphorylation. Mitochondrial ATP production is sensitive to intra-mitochondrial free $[Ca^{2+}]$ ($[Ca^{2+}]_{mito}$) as several key enzymes of the Krebs cycle and the

Corresponding author: Donald M. Bers, Department of Pharmacology, University of California Davis, Genome Building 3511, Davis, CA 95616-8636, Email: E-mail: dmbers@ucdavis.edu, Tel: 1-(530) 752-6517, FAX: 1- (530)-752-7710.

F_1F_oATPase are activated by micromolar Ca^{2+} [1]. $[Ca^{2+}]_{mito}$ may therefore provide important feedback between cellular energy demand and supply, especially when increased cardiac inotropy is mediated by increased $[Ca^{2+}]_i$ (e.g. during beta-adrenergic stimulation) [2]. Numerous participants and regulators of mitochondrial Ca^{2+} in- and efflux contribute to the complex regulation of $[Ca^{2+}]_{mito}$ which is important to maintain cellular function [3].

Ca^{2+} influx into mitochondria occurs via the mitochondrial Ca^{2+} uniporter (mCU), a low affinity ($K_{0.5}$ ~tens of micromolar), high capacity uptake mechanism which utilizes the large electrochemical gradient for Ca^{2+} across the inner mitochondrial membrane [3]. So far, the molecular entity of the mCU has not been identified, but was recently functionally characterized as an inwardly rectifying Ca^{2+}-selective channel [4]. Additionally, mitochondrial Ca^{2+} uptake has been proposed to occur via a rapid mode of Ca^{2+} uptake (RaM) [5] and via mitochondrial ryanodine receptors [6]; however, the contribution of these putative mechanisms to the regulation of $[Ca^{2+}]_{mito}$ in cardiomyocytes is unclear.

The low Ca^{2+} affinity of the mCU may limit Ca^{2+} entry during diastole and normal Ca^{2+} transients (where spatially averaged $[Ca^{2+}]_i$ is 0.1 – 1 μM). However, because parts of mitochondria are in close spatial proximity to sarcoplasmic reticulum (SR) Ca^{2+} release sites, the local $[Ca^{2+}]_i$ near ryanodine receptors or IP_3-receptors may greatly exceed bulk $[Ca^{2+}]_i$ allowing more rapid mitochondrial Ca^{2+} uptake via mCU [7].

Mitochondrial Ca^{2+} efflux occurs predominantly in a Na^+-dependent manner ($K_{0.5}$~4–10 mM) via the mitochondrial Na^+/Ca^{2+}-exchanger (NCX_m) [8]. Mitochondrial Ca^{2+} regulation is therefore sensitive to variations in cytosolic $[Na^+]$ ($[Na^+]_i$) which may occur during ischemia/reperfusion [9] or during heart failure [10]. Although Na^+-independent mitochondrial Ca^{2+} efflux has been proposed [11], in the heart its contribution to $[Ca^{2+}]_{mito}$ seems negligible [12].

It is well established that cardiac mitochondria can take up a small fraction of the cytosolic Ca^{2+} involved in excitation-contraction (EC) coupling [8,13], potentially shaping cellular Ca^{2+} signals [14]. However, two aspects remain unclear and controversial. First, it is unresolved whether $[Ca^{2+}]_{mito}$ rapidly follows the beat-to-beat variations of $[Ca^{2+}]_i$ or whether $[Ca^{2+}]_{mito}$ changes slowly, integrating variations in $[Ca^{2+}]_i$ over many beats [8,15]. Second, $[Ca^{2+}]_{mito}$ measurements have generally not been calibrated, making it difficult to know how large the $[Ca^{2+}]_{mito}$ transients are and how important the phasic $[Ca^{2+}]_{mito}$ signals are relative to Ca^{2+} fluxes during EC-coupling.

In this study, we investigated calibrated mitochondrial $[Ca^{2+}]$ changes in response to both steady changes in $[Ca^{2+}]_i$ (in heavily buffered solution) and in response to SR Ca^{2+} release in permeabilized rat ventricular cardiomyocytes. During SR Ca^{2+} release, $[Ca^{2+}]_{mito}$ rises rapidly with a delay after the $[Ca]_i$ rise, but shows much slower decline, resulting in beat-to-beat integration. During steady-state SR Ca^{2+} releases, mitochondrial Ca^{2+} uptake is small and Ca^{2+} influx and efflux are balanced. The amplitude of the $[Ca^{2+}]_{mito}$ transient during an individual $[Ca^{2+}]_i$ transient is less than 10 nM. These data provide novel insights into mitochondrial Ca^{2+} regulation in cardiac myocytes.

Methods

Cardiac myocyte preparation, dye loading and cell permeabilization

Cardiac ventricular myocytes were isolated from adult male Sprague-Dawley rats (250–300 g) using protocols approved by the UC Davis Institutional Animal Care and Use Committee (IACUC) (see Online Supplement for details). Freshly isolated cells were plated on laminin-

coated glass cover slips for at least 45 min before dye loading. All experiments were performed at room temperature (RT) (22–23°C).

Cells were loaded with 10 μM fura-2 AM for 45 min or with rhod-2 AM for 30 min at RT in nominally Ca^{2+} free Tyrode's solution (in mM: HEPES 5, NaCl 140, KCl 4, $MgCl_2$ 1, glucose 10; pH adjusted to 7.4 with NaOH). 30 min were allowed for de-esterification. Before permeabilization the bath solution was changed to a Na^+-free/Ca^{2+}-free Tyrode's solution (in mM: HEPES 10, tetraethylammonium chloride 140, KCl 4, $MgCl_2$ 1, EGTA 2, glucose 10; pH adjusted to 7.4 with Trisma base) for 3–5 min. The cell surface membrane was permeabilized with saponin by exposure to a solution containing 50 μg/mL saponin and (in mM) HEPES 10, K-aspartate 135, $MgCl_2$ 0.7, EGTA 2, reduced glutathione 10, MgATP 5, glucose 10 for 30 s or less.

Solutions

A highly Ca^{2+}-buffered, Ca^{2+}-free, Na^+-free internal solution contained (in mM): EGTA 5, HEPES 20, K-aspartate 100, KCl 40, $MgCl_2$ 1, maleic acid 2, glutamic acid 2, pyruvic acid 5, KH_2PO_4 0.5, BDM 15, pH 7.2 adjusted with trisma base. To control $[Ca^{2+}]_i$, 1.00 M $CaCl_2$ solution (Fluka, #21115) was added as calculated with Max-Chelator (http://www.stanford.edu/~cpatton/maxc.html). Free $[Ca^{2+}]$ was confirmed by Ca^{2+}-sensitive electrode measurements. Na^+-free internal solution with low Ca^{2+} buffering capacity and 150 nM free $[Ca^{2+}]$ contained (in mM): EGTA 0.05, $CaCl_2$ 0.0234, HEPES 20, K-aspartate 100, KCl 40, $MgCl_2$ 0.551, maleic acid 2, glutamic acid 2, pyruvic acid 5, KH_2PO_4 0.5, MgATP 5, reduced glutathione 10, pH 7.2 adjusted with trisma base. When NaCl was added to these solutions, equal amounts of KCl were omitted. Calibration solutions contain 2–3 μM ionomycin, 10 μM FCCP and 20 μg/mL oligomycin.

Fluorescence microscopy

Fura-2 fluorescence was measured (Nikon DIAPHOT 200, 40× oil-immersion objective) with excitation at 345±10 and 380±5 nm (F_{340} and F_{380}), with emission at 505±50 nm. The signals were corrected for background and autofluorescence by subtracting averaged signals from unloaded cells (n=6, determined every day). Autofluorescence (unloaded cell signal minus empty field signal) is ≤10% of background corrected Fura-2 signals. Laser scanning confocal microscopy (Zeiss, LSM5 Pascal, 40× water immersion objective) was used for imaging. For mitochondrial localization Fura-2 was loaded as above and 500 nM Mitotracker Orange was included during de-esterification. Fura-2 and Mitotracker Orange were excited sequentially at 405 nm (diode laser) and 453 nm (helium-neon laser) with emission at 505–530 nm and 560–615 nm bandpass filters, respectively. Mitochondrial Rhod-2 fluorescence was measured with the same confocal microscope (543 nm excitation, emission >560 nm) as 2-dimensional images or in line-scan mode (786 ms/frame and 3–26 ms/line). In some rhod-2 experiments, $[Ca^{2+}]_i$ was measured simultaneously with $[Ca^{2+}]_{mito}$ using 2 or 5 μM K_5fura-2 in the internal solution (405 nm excitation, 505–530 nm emission). In permeabilized cells not loaded with rhod-2/AM, 50% of the fura-2 fluorescence intensity measured at 505–530 nm was detected in the rhod-2 window (>560 nm), contaminating the rhod-2 signal. The corrected rhod-2 signal is $F_{543}^{corr} = F_{543} + (F_{405}^0 - F_{405})/2$, where F_{543} is the raw rhod-2 fluorescence, F_{405}^0 is the resting fura-2 signal and F_{405} is the fura-2 signal (which decreases during Ca^{2+} transients).

A Ca^{2+}-insensitive, isosbestic signal (F_c) was calculated from the Ca^{2+}-sensitive fluorescence signals as described by Zhou & Neher [16] (see Results and Online Supplement). In situ calibration of mitochondrial fura-2 was performed (see Fig. 2C-D and Online Supplement for details) using 2–3 μM ionomycin, 10 μM FCCP and 20 μg/mL oligomycin to allow $[Ca^{2+}]_i$ - $[Ca^{2+}]_{mito}$ equilibration. This allowed transformation of mitochondrial fura-2 signals to $[Ca^{2+}]_{mito}$.

Drugs and Statistics

Indicators were obtained from Invitrogen (Eugene, OR), Ru360, CGP-37157 from CALBIOCHEM (La Jolla, CA) and other chemicals from Sigma (St. Louis, MO). Data are presented as mean ± SD of n measurements. Comparison between groups was performed with One-Way ANOVA (significant at $P < 0.05$).

Results

Mitochondrial free [Ca^{2+}] measurements in rat myocytes

To measure calibrated $[Ca^{2+}]_{mito}$ in isolated ventricular rat cardiomyocytes we used the ratiometric Ca^{2+} indicator fura-2 under conditions promoting mitochondrial fura-2 loading, and removed cytosolic indicator by permeabilization. Saponin-induced permeabilization allows tight control of the cytosolic milieu (e.g. free $[Ca^{2+}]$, $[Na^+]$, Ca^{2+}-buffering capacity) while allowing periodic SR Ca^{2+} release when desired.

Figure 1A shows confocal images of an intact cardiomyocyte after loading with fura-2 (Fig. 1Aa, green) and mitochondrial staining with Mitotracker Orange (Fig. 1Ab, red). Saponin permeabilization (Fig. 1B) did not appreciably alter the characteristic mitochondrial pattern with Mitotracker Orange, but washed out most of the fura-2, leaving residual fura-2 matching the mitochondrial pattern.

To measure the fraction of total fura-2 loading that was mitochondrial, we used the Ca^{2+}-insensitive fura-2 fluorescence (F_c) before and after permeabilization (Fig. 2A). F_c was calculated $F_c = F_{340} + \alpha F_{380}$, where $-\alpha$ is the slope of the F_{340} vs. F_{380} curve when $[Ca^{2+}]_{mito}$ changes (top parts of Fig. 2A, where $[Ca^{2+}]_{mito}$ was altered by raising $[Ca^{2+}]_i$ from 0 to 429 nM). The F_c trace in Fig. 2A shows that saponin permeabilization released 70% of the total fura-2 loaded into the intact myocyte (note that F_c did not change with $[Ca^{2+}]_{mito}$). The remaining 30% of fura-2 was compartmentalized in mitochondria. The stability of F_c after permeabilization indicates no substantial mitochondrial fura-2 leakage over 30 min.

To confirm that the measured fura-2 fluorescence reflect $[Ca^{2+}]_{mito}$, we applied the protonophore FCCP (2.5 μM) to dissipate the mitochondrial membrane potential (Ψ_m) and therefore the driving force for the mitochondrial Ca^{2+} uniporter (the main mitochondrial Ca^{2+} influx pathway). Figure 2B shows that FCCP abolished the rise in fura-2 ratio induced by raising $[Ca^{2+}]_i$ to 800 nM (in Na^+-free solution). This demonstrates that the fura-2 fluorescence changes under our conditions depend on an intact Ψ_m and are therefore a valid measure of $[Ca^{2+}]_{mito}$.

Since fluorescent indicator properties can depend on environment [17] we performed in situ calibration of mitochondrially compartmentalized fura-2 in rat ventricular myocytes (Fig. 2C–D). Myocytes were equilibrated with solutions of different $[Ca^{2+}]$ (0–95 μM containing Ca^{2+} ionophore ionomycin (3 μM), the protonophore FCCP (10 μM) to collapse Ψ_m, and oligomycin (20 μg/mL) to inhibit the F_1F_oATP-synthase). We found an in situ K_d of 170 nM in this experiment and results were very consistent among cells (K_d = 170±0.3 nM, n = 3).

Steady-state dependence of $[Ca^{2+}]_{mito}$ on cytosolic [Ca^{2+}]

Next, we determined the steady-state dependence of $[Ca^{2+}]_{mito}$ on the $[Ca^{2+}]_i$ in the presence of 10 mM $[Na^+]_i$ with Ca^{2+} buffered by 5 mM EGTA. This EGTA concentration allows the precise control of $[Ca^{2+}]_i$ and prevents spontaneous SR Ca^{2+} releases (which are examined below). The internal solution contained no ATP or ADP and contained 15 mM BDM to avoid cell contraction at high $[Ca^{2+}]_i$.

Fig. 3A shows background corrected F_{340} and F_{380} immediately after permeabili-zation (at 3 min in Fig. 3A), in Ca^{2+}-free internal solution (10 min) followed by 10 min at 429 nM $[Ca^{2+}]_i$. After reaching steady-state, a two point calibration was performed using Ca^{2+}-free and high $[Ca^{2+}]_i$ solution (50–100 μM) with ionomycin (3 μM), oligomycin (20 μg/mL), and FCCP (10 μM) to determine R_{min}, R_{max}, $F_{380\text{-}max}$ and $F_{380\text{-}min}$. Using these and the measured in situ K_d, the fura-2 fluorescence was transformed into $[Ca^{2+}]_{mito}$ (Fig. 3B; using the equation in Fig. 2D legend). Figure 3C shows the steady-state $[Ca^{2+}]_{mito}$ vs. $[Ca^{2+}]_i$ relationship. Below an apparent threshold of ~300 nM $[Ca^{2+}]_i$, $[Ca^{2+}]_{mito}$ had a very shallow dependence on $[Ca^{2+}]_i$ and increased only very little as $[Ca^{2+}]_i$ increased. At cytosolic $[Ca^{2+}]$ > ~300 nM, $[Ca^{2+}]_{mito}$ showed a steep dependence on $[Ca^{2+}]_i$ and exceeded $[Ca^{2+}]_i$ for $[Ca^{2+}]_i$ > 500 nM.

Mitochondrial $[Ca^{2+}]$ uptake during spontaneous SR Ca^{2+} release

While these steady-state measurements provide a solid foundation, we next sought to test how $[Ca^{2+}]_{mito}$ changes during phasic SR Ca^{2+} release events which may better mimic mitochondrial Ca^{2+} regulation *in vivo*. By reducing [EGTA] to 50 μM and with $[Ca^{2+}]_i$ =150 nM (and physiological internal solution) spontaneous SR Ca^{2+} release events (Ca^{2+} waves) occurred at a regular frequency of 5–15 min^{-1}.

Fig. 4A shows a typical continuous $[Ca^{2+}]_{mito}$ recording (gray trace) and cell contraction (black trace) starting after permeabilization. For this experiment, $[Na^+]_i$ was 15 mM and 40 μM Cytochalasin-D was added to reduce, but not abolish cell contraction during cytosolic Ca^{2+} waves. The small residual contractions were used to measure SR Ca^{2+} wave occurrence. The inset in Fig. 4A shows a $[Ca^{2+}]_{mito}$ transient with curve-fit and cell contraction. Because the fura-2 loaded cardiomyocytes were incubated in Ca^{2+}-free solution before permeabilization and permeabilized in Ca^{2+}-free internal solution, $[Ca^{2+}]_{mito}$ was very low at the beginning of the measurement. $[Ca^{2+}]_{mito}$ was stable at ~57nM during the first 10 sec before the first Ca^{2+} wave occurred. The first 3 contractions after permeabilization in Fig. 4A were associated with step-wise increases in $[Ca^{2+}]_{mito}$ without substantial mitochondrial Ca^{2+} extrusion. Only in subsequent Ca^{2+} transients did mitochondrial Ca^{2+} extrusion become evident (as a declining phase of $[Ca^{2+}]_{mito}$). $[Ca^{2+}]_{mito}$ gradually increased to ~110 nM after 8 waves and to 216 nM after 20 waves. Control experiments using TMRM to assess Ψ_m, showed no appreciable change in Ψ_m during the phasic or integrated rise in $[Ca^{2+}]_{mito}$.

To test whether SR Ca^{2+} release was responsible for this dynamic $[Ca^{2+}]_{mito}$ uptake we inhibited SR function (Fig. 4B–D). To limit cellular photo damage and allow long-term $[Ca^{2+}]_{mito}$ measurements over 20 min, we measured $[Ca^{2+}]_{mito}$ every 15 s for a duration of 2 s (each point in Fig. 4B–E is average $[Ca^{2+}]_{mito}$ during the 2 s).

Fig. 4B shows that blocking SR Ca^{2+} uptake by pretreatment with the specific SR Ca^{2+}ATPase (SERCA) inhibitor thapsigargin (1 μM for 30 min before permeabilization to deplete SR Ca^{2+}) nearly abolished the rise in $[Ca^{2+}]_{mito}$. Under these conditions no spontaneous SR Ca^{2+} release events occurred and the small residual rise in $[Ca^{2+}]_{mito}$ to ~54 nM is explained by the slow steady-state equilibration at the ambient 150 nM $[Ca^{2+}]_i$ (in this case with $[Na^+]_i$=0 which inhibits NCX_m). Figure 4C–D shows that either acute SR Ca^{2+} depletion with 10 mM caffeine or inhibition of SR Ca^{2+} release by 2 mM tetracaine terminated the $[Ca^{2+}]_{mito}$ rise abruptly. Notably, in both cases Ca^{2+} waves ceased, but $[Ca^{2+}]_{mito}$ failed to decline in the Na^+-free solution ($[Ca^{2+}]_{mito}$ declines less than 5 nM/min, n=3), consistent with a dominant role of NCX_m in mitochondrial Ca^{2+} extrusion. Selective blockade of the mitochondrial uniporter with Ru360 (Fig. 4E) also stopped the rise in $[Ca^{2+}]_{mito}$, although spontaneous cytosolic Ca^{2+} waves continued.

These results demonstrate that the observed mitochondrial Ca^{2+} uptake occurs as a direct consequence of SR Ca^{2+} release (we maintain the structural organization of the cardiac

myocyte regarding the crosstalk between the SR and mitochondria), and that the major Ca^{2+} influx pathway under these conditions is the mitochondrial Ca^{2+} uniporter.

Quantitative analysis of the rise of $[Ca^{2+}]_{mito}$ per beat

In Figures 4C and 4D $[Ca^{2+}]_{mito}$ failed to decline in Na^+-free solution after Ca^{2+} transients were blocked by caffeine or tetracaine. Figure 5A shows that with 15 mM $[Na^+]_i$, caffeine still abruptly stopped the rise in $[Ca^{2+}]_{mito}$ (filled circles), but $[Ca^{2+}]_{mito}$ then declined exponentially (τ=3.4 min) to reach the same level as seen in the steady-state measurement protocol (with the same $[Na^+]_i$, open circles). This shows that mitochondrial Ca^{2+} is removed effectively via a Na^+-dependent pathway when mitochon-drial Ca^{2+} uptake is stopped.

Figure 5B shows representative experiments monitoring the rise in $[Ca^{2+}]_{mito}$ and the number of spontaneous contractions (±15 mM $[Na^+]_i$). In the absence of $[Na^+]_i$ the $[Ca^{2+}]_{mito}$ rose linearly until the calibration was initiated. In contrast, with 15 mM $[Na^+]_i$, the $[Ca^{2+}]_{mito}$ increased linearly initially, but then reached a steady-state within ~15 min. This demonstrates that Na^+-dependent $[Ca^{2+}]_{mito}$ removal is required to allow $[Ca^{2+}]_{mito}$ to reach a steady-state during regular SR Ca^{2+} release. The rise in $[Ca^{2+}]_{mito}$ per SR Ca^{2+} release ($\Delta[Ca^{2+}]_{mito}$/wave) can be calculated from the linear part of the uptake measurements. The rate of $[Ca^{2+}]_{mito}$ rise in the absence and presence of Na^+ during the indicated 35 and 17 beats in Fig. 5B was 3.1 and 1.8 nM/wave, respectively. Mean data in Fig. 5C show this rise in $[Ca^{2+}]_{mito}$/wave to be 3.6±1.5 nM (n=16) and 2.2±1.1 nM (n=19) in the absence and presence of 15 mM $[Na^+]_i$, respectively.

Figure 5D shows that abrupt block of the NCX_m with 5 μM CGP-37157 during the rising phase of $[Ca^{2+}]_{mito}$ with 15 mM $[Na^+]_i$ increased the rate of rise of $[Ca^{2+}]_{mito}$ per wave. The mean acceleration induced by CGP-37157 in 4 cells was 74%, similar to the 63% higher rate of $[Ca^{2+}]_{mito}$ rise per wave in Na^+-free solution in Fig. 5C.

Spatially resolved $[Ca^{2+}]_{mito}$ measurements during SR Ca^{2+} release

The above calibrated $[Ca^{2+}]_{mito}$ measurements with fura-2 and measures of $[Ca^{2+}]_{mito}$ rise per Ca^{2+} wave allows us to extend these studies with additional spatio-temporal detail using confocal microscopy and the cationic fluorescent Ca^{2+} indicator rhod-2 (which is less readily calibrated). Figure 6A shows a rhod-2 loaded cardiomyocyte 5 min after permeabilization after $[Ca^{2+}]_{mito}$ has risen by ~50 nM (see Fig. 6B). The movie (in Online Supplement) shows the pulsatile emergence of the clear mitochondrial pattern as $[Ca^{2+}]_{mito}$ and rhod-2 fluorescence rise. We focused our analysis on intermyofibrillar mitochondria because some subsarcolemmal mitochondria were less consistent.

Figure 6B shows mitochondrial fluorescence during Ca^{2+} waves (5–6 min^{-1}) from two large regions of interest (ROI1 and 2 in Fig. 6A) at opposite ends of the cell. As in Fig. 4A, $[Ca^{2+}]_{mito}$ increased during the first transients in a step-like manner without appreciable $[Ca^{2+}]_{mito}$ decay. The rhod-2 fluorescence changes in ROI 1 and ROI 2 were very similar (and like the whole cell), suggesting that $[Ca^{2+}]_{mito}$ is relatively homogeneous when a large fraction of the cellular mitochondria is compared. Additionally, the $[Ca^{2+}]_{mito}$ peaks in ROI 1 and 2 were within 1 s of each other, indicating relatively homogeneous cytosolic Ca^{2+} changes.

Using the $[Ca^{2+}]_{mito}$ gain per Ca^{2+} wave measured with fura-2 (2.2 nM/wave; Fig. 5C), we infer that the $[Ca^{2+}]_{mito}$ rise for the 13 transients indicated was 28.6 nM for both ROI 1 and ROI 2. This indicates that one fluorescence unit reflects a $\Delta[Ca^{2+}]_{mito}$ of ~1.44 nM $[Ca^{2+}]_{mito}$. Next, we used this approximation to estimate $[Ca^{2+}]_{mito}$ changes in two smaller ROIs (Fig. 6C, ROI 3 and 4 shown in Fig. 6A). These smaller ROIs (with only 3 mitochondria) differed slightly. ROI 3 showed a linear increase much like ROI 1 and 2, whereas $[Ca^{2+}]_{mito}$

in ROI 4 reached a plateau after gaining ~60 nM in 3 min. The upstroke amplitudes of individual $[Ca^{2+}]_{mito}$ transients in the inset of Fig. 6C were ~10–12 nM (for the 3 indicated transients). These results suggest that individual mitochondria or small clusters of mitochondria can respond differently to a homogenous cytosolic Ca^{2+} transient and that the amplitudes of $[Ca^{2+}]_{mito}$ transients are much smaller (~100x) than the amplitude of bulk cytosolic Ca^{2+} transients.

Kinetics of $[Ca^{2+}]_{mito}$ changes during SR Ca^{2+} release

To enhance temporal resolution, we used line-scan confocal microscopy along a 40.5 μm line (~20 mitochondria). Figure 7A shows $[Ca^{2+}]_{mito}$ which rose to a steady-state within a small number of Ca^{2+} waves (expanded time scale in Fig. 7B; typical of 5 other cells). Figure 7Ab shows the $[Ca^{2+}]_{mito}$ rise and fall amplitudes for each beat. The first $[Ca^{2+}]_{mito}$ transient had a large upstroke and small decline amplitude, leading to a large rise in $[Ca^{2+}]_{mito}$ with little decay in $[Ca^{2+}]_{mito}$ (Fig. 7B#1). As mitochondria gained Ca^{2+} (Fig. 7Ad), upstroke amplitudes decreased and decline amplitudes increased until influx and efflux balanced (Fig. 7B#6 and #11) and $[Ca^{2+}]_{mito}$ stopped increasing. The time constant of $[Ca^{2+}]_{mito}$ decay was typically 2.5–5 s (Fig. 7B). At steady-state, $[Ca^{2+}]_{mito}$ transients were very small. Thus, mitochondria can rapidly follow cytosolic $[Ca^{2+}]$ changes when $[Ca^{2+}]_{mito}$ is low, but during steady-state, $[Ca^{2+}]_{mito}$ does not change appreciably in response to cytosolic Ca^{2+} transients.

In the next experiments, we compared the kinetics of $[Ca^{2+}]_{mito}$ and $[Ca^{2+}]_i$ transients, simultaneously measured with mitochondrial rhod-2 and cytosolic fura-2 using the confocal line-scan mode (fura-2 salt was in the cytosolic solution). Figure 8A shows a typical experiment starting 40 s after permeabilization (with expanded traces in Fig. 8B with fura-2 signal inverted). The $[Ca^{2+}]_i$ signals in Fig. 8 were not calibrated, but parallel calibrated experiments with the same protocol showed Ca transients of 1.3–2.5 μM (i.e. typical of spontaneous waves in intact myocytes). Time-to-peak for $[Ca^{2+}]_{mito}$ and $[Ca^{2+}]_i$ transients is shown in Fig. 8Ab (note that this is the rise time for each trace independently). The delay between the $[Ca^{2+}]_i$ and $[Ca^{2+}]_{mito}$ peaks (peak-to-peak) and start-to-start delays are shown in Fig. 8Ac.

Figure 8B shows that $[Ca^{2+}]_i$ transients preceded $[Ca^{2+}]_{mito}$ transients. On average, $[Ca^{2+}]_i$ started to rise 111±60 ms before $[Ca^{2+}]_{mito}$. $[Ca^{2+}]_i$ rose to peak in 213±59 ms, whereas $[Ca^{2+}]_{mito}$ rose slightly slower (in 275±86 ms, $p<0.05$, n =25 transients, 3 cells, Fig. 8C). Due to the later start and the slower upstroke, $[Ca^{2+}]_{mito}$ peaked 177±72 ms after $[Ca^{2+}]_i$ (Fig. 8C). $[Ca^{2+}]_{mito}$ decline was dramatically slower than $[Ca^{2+}]_i$ decline (time constant were 2.8±0.7 s vs. 0.19±0.06 s, respectively, Fig. 8C). Additionally, the time constant of $[Ca^{2+}]_{mito}$ decline was relatively constant from transient-to-transient suggesting that extrusion was not activated by increasing $[Ca^{2+}]_{mito}$ (Fig. 8Ad).

Discussion

Cardiac mitochondrial Ca^{2+} uptake may be important in controlling energy supply-demand balance (via activation of mitochondrial dehydrogenases), protecting myocytes from transient Ca^{2+} overload and mediating cell death pathways (necrosis or apoptosis) [14,18–20]. Mitochondrial Ca^{2+} uptake occurs in response to elevated $[Ca^{2+}]_i$ (which in heart occurs transiently with each beat) and it is increasingly clear that some Ca^{2+} enters the mitochondria with each heartbeat [21–25]. However, most prior studies of $[Ca^{2+}]_{mito}$ in cardiac myocytes lack calibration, and in some cases contamination of the $[Ca^{2+}]_{mito}$ signal by cytosolic indicator has not been completely ruled out. These aspects limit the quantitative understanding of mitochondrial Ca^{2+} regulation, and motivated the present study. Here we show carefully calibrated $[Ca^{2+}]_{mito}$ signals in permeabilized cardiac myocytes both at rest (where we characterized the steady-state $[Ca^{2+}]_{mito}$ vs. $[Ca^{2+}]_i$ relationship) and during regular SR Ca^{2+} release events. We find that the largest rise in $[Ca^{2+}]_{mito}$ during a local SR Ca^{2+} release

is ~10 nM (e.g. when $[Ca^{2+}]_{mito}$ begins very low), and the rise occurs rapidly (275 ms time to peak) within a 100–200 ms delay of the rise in $[Ca^{2+}]_i$. However, the $[Ca^{2+}]_{mito}$ decline is ten times slower than that of $[Ca^{2+}]_i$ (2.8 vs. 0.19 s time constant). The slow $[Ca^{2+}]_{mito}$ decline between beats leads to integration of $[Ca^{2+}]_{mito}$ (even at the low frequency of spontaneous Ca^{2+} waves here) to a level many times higher than the amplitude of a single $[Ca^{2+}]_{mito}$ transient. While we acknowledge that these myocytes are not in a truly physiological setting, these results provide useful novel quantitative data to help understanding mitochondrial Ca^{2+} balance in cardiac myocytes.

Limitations

We have measured $[Ca^{2+}]_{mito}$ in quantitative detail in a relatively physiological mitochondrial environment using saponin-permeabilized myocytes, selective mitochon-drial ratiometric Ca^{2+} indicator and intrinsic spontaneous large SR Ca^{2+} release events [26–28]. However, the control gained by permeabilization makes the situation less physiological in several ways. First, small diffusible molecules may be lost by the myocyte, and we cannot rule out that this could alter regulation of mitochondrial Ca^{2+} transport mechanisms (although the impact of this is unknown). Second, it is possible that the saponin exposure changes the physical geometry between the SR Ca^{2+} release junctions and the mitochondria. While we have no reason to expect this, it also cannot be ruled out. Third, and perhaps most important, we are limited in the frequency of SR Ca^{2+} release events, to that which occurs spontaneously (up to ~0.2 Hz). This is much lower than the frequency of the normal heartbeat (even at our sub-physiological 23°C). At higher frequencies, we would expect more dramatic $[Ca^{2+}]_{mito}$ integration (i.e. $[Ca^{2+}]_{mito}$ would rise higher at steady-state), but we do not expect that would increase the transient $\Delta[Ca^{2+}]_{mito}$ associated with a single SR Ca^{2+} release. Indeed, the phasic components might be expected to be smaller at higher $[Ca^{2+}]_{mito}$ in the steady-state (as in cases here as the steady-state is approached in Fig. 7 and 8). Fourth, the spontaneous SR Ca^{2+} releases occur as propagated waves (which travel at ~100 μm/s) through the cytosol. While this will spread out the time course of $[Ca^{2+}]_i$ and $[Ca^{2+}]_{mito}$ kinetics, it should do so in a parallel manner, such that relative comparisons are still well justified. Furthermore, our most critical kinetic analysis is done in local regions containing 3–30 mitochondria, where this concern is less of a limitation. One might also wonder if the local SR Ca^{2+} release during these waves may be less than during physiological Ca^{2+} transients. However, these events occur only at high SR Ca^{2+} loads, and if anything are likely to be higher at the local level than the normal physiological Ca^{2+} transient [29]. On the other hand, using permeabilized cells allows the measurement of purely mitochondrially derived fluorescence without having to deal with potential problems associated with Mn^{2+}-quench (e.g. inhibition of the mitochondrial Ca^{2+} transport or inhibition of oxidative phosphorylation by Mn^{2+}) [3,30], an approach which has been used to minimize cytosolic fluorescence [31,32]. Thus, while trade-offs are required for the quantitative confidence we have in our results, this work is highly relevant for understanding physiological mitochondrial Ca^{2+} regulation.

Quantitative changes in $[Ca^{2+}]_{mito}$

Our experiments start from Ca^{2+} depleted mitochondria, because of pre-incubation in low $[Ca^{2+}]_o$ prior to permeabilization and permeabilization in Ca^{2+}-free solution. Starting from this low level, we see the largest increases of $[Ca^{2+}]_{mito}$ during the first several Ca^{2+} transients. Note that the $[Ca^{2+}]_i$ signals usually do not change appreciably (see Fig. 8A), so the change in $[Ca^{2+}]_{mito}$ transients is not secondary to $[Ca^{2+}]_i$ transient differences. The first few $[Ca^{2+}]_{mito}$ transients have the largest rising phases and often exhibit little decline (consistent with little Ca^{2+} efflux at very low $[Ca^{2+}]_{mito}$). Indeed, some of the slight decline in $[Ca^{2+}]_{mito}$ in the first transient in Fig. 8 might be due to buffering of $[Ca^{2+}]_{mito}$. Notably, the rising phase of $[Ca^{2+}]_{mito}$ becomes much smaller (almost 10 times, Fig. 8Ab) as integrated $[Ca^{2+}]_{mito}$ approaches steady-state. This might be partly due to faster Ca^{2+} extrusion as

$[Ca^{2+}]_{mito}$ rises. However, because the Ca^{2+} efflux kinetics are so slow (τ=2.8 s even at higher $[Ca^{2+}]_{mito}$, Fig. 8Ad), speeding efflux by 2-fold should only reduce amplitude <10%. Thus the reduced amplitude may also reflect reduced Ca^{2+} influx (although the mechanism is not obvious). We also showed that NCX_m is required for Ca^{2+} efflux from mitochondria. $[Na^+]_i$ was held constant here at 15 mM, but when $[Na^+]_i$ changes physiologically this would be expected to alter the steady-state $[Ca^{2+}]_{mito}$ and rate of $[Ca^{2+}]_{mito}$ decline [23,33]. In any event, at steady-state (where $[Ca^{2+}]_{mito}$ stops rising) influx and efflux must be the same and both appear to be much lower than the maximal rising phase of $[Ca^{2+}]_{mito}$ when influx starts.

The maximal rise of $[Ca^{2+}]_{mito}$ during a single SR Ca^{2+} release is ~10 nM (Fig. 6C) with typical rise values of 2–4 nM (Fig. 5D). If we assume that intra-mitochondrial Ca^{2+} buffering is 100:1 (as in cytosol), and use the highest value (10 nM) this would translate to 1 μM rise in total mitochondrial Ca^{2+} content, which corresponds to removal of 0.5 μmol/l cytosol. Surprisingly, this agrees well with Bassani et al. estimates of the quantitative contribution of mitochondrial Ca^{2+} uptake to removal of cytosolic Ca^{2+} during E-C coupling by analysis of $[Ca^{2+}]_i$ decline by different Ca^{2+} transporters in intact rat ventricular myocytes [13]. They found that ~75 μmol/l cytosol of Ca^{2+} were added and removed to the cytosol at a normal Ca^{2+} transient, and that about 1% was removed by the combination of mitochondria plus sarcolemmal Ca^{2+}-ATPase (0.8 μmol/l cytosol) which contribute about equally with each other [34]. Given the completely different methods and limitations, the quantitative agreement encourages us to think we are close to correct.

Local vs. global $[Ca^{2+}]_i$ drives mitochondrial Ca^{2+} uptake

Several studies have suggested that mitochondria are in close physical proximity to the sites of SR Ca^{2+} release and consequently that SR (or endoplasmic reticulum) Ca^{2+} release has preferential access to drive mitochondrial Ca^{2+} uptake [7,35–39]. Indeed, Sharma *et al.* [36] showed that 1 mM BAPTA (a fast Ca^{2+} buffer), which reduced the caffeine-induced rise in $[Ca^{2+}]_i$ by 90% in permeabilized rat myocytes, only decreased the mitochondrial rhod-2 signal by 23%. Our results are consistent with this general idea and provide some quantitative context in terms of $[Ca^{2+}]_{mito}$. Note that when we abruptly switch bath $[Ca^{2+}]$ from 0 to 429 nM (heavy $[Ca^{2+}]_i$ buffering; Fig. 3B) or pretreat myocyte with thapsigargin (Fig. 4B) the rate of $[Ca^{2+}]_{mito}$ rise is linear over several minutes (0.1–0.7 nM/s). This is much slower than during an SR Ca^{2+} release 36 nM/s (10 nM/0.275 s), where global $[Ca^{2+}]_i$ is only transiently raised to a slightly higher level (0.5–1 μM $[Ca^{2+}]_i$). This suggests that phasic mitochondrial Ca^{2+} influx must be driven in large part by the higher local (vs. global) $[Ca^{2+}]_i$ during SR Ca^{2+} release. This makes sense with the high $K_{0.5}$ for $[Ca^{2+}]_i$ of the mCU [3], which is required for the observed mitochondrial Ca^{2+} uptake seen here. We can look at this another way. The 20 Ca^{2+} waves during the 2 min in Fig. 4A only raise average $[Ca^{2+}]_i$ from 150 to 200 nM (assuming each has peak $[Ca^{2+}]_i$ ~1 μM with kinetics as in Fig. 8). Based on the data in Fig. 3C and with thapsigargin in Fig. 4B, this small rise in global $[Ca^{2+}]_i$ alone could not increase $[Ca^{2+}]_{mito}$ to 200 nM. So the SR Ca release events are clearly important drivers of $[Ca^{2+}]_{mito}$ rise.

Two points should be borne in mind here. First, while high local SR Ca^{2+} release accelerates mitochondrial Ca^{2+} uptake, the total amount is still small compared to SR Ca^{2+} uptake or Na^+/Ca^{2+} exchange in cardiac myocytes [13]. Second, while one end of a large mitochondrion may be close to the site of SR Ca^{2+} release (e.g. 37–270 nm; [36]) the other end of a typical intramyofibrillar mitochondrion is ~1 μm away, at the middle of the sarcomere. Considering the overall mitochondrial geometry, the average place on the mitochondrion within the sarcomere probably senses a similar local $[Ca^{2+}]_i$ as does the cytosol. Thus, there may be preferential local Ca^{2+} influx on the end of a mitochondrion that is very close to an SR Ca^{2+}

release unit, but this may be diluted and buffered strongly in the whole mitochondrion. Sub-mitochondrial $[Ca^{2+}]_{mito}$ gradients might even exist, at least transiently.

Phasic vs. integrative signaling

Our $[Ca^{2+}]_{mito}$ dependence on $[Ca^{2+}]_i$ in highly buffered solutions agrees fairly well with and validates the classical studies in isolated mitochondria [40] and of Miyata *et al.* [31] who used Mn^{2+} to quench cytosolic indo-1 during slow Ca^{2+} transients mediated by Na^+/Ca^{2+} exchange (rather than SR Ca^{2+} release; compare our Fig. 3C with their Fig. 7B). Thus, Fig. 3C represents well the static quasi-equilibrium relationship. It seems clear that Fig. 3C is a good representation of the static quasi-equilibrium relationship. While helpful, this alone does not inform the question of dynamic $[Ca^{2+}]_{mito}$ regulation during SR Ca^{2+} release.

Experimental data in favor of both "slow integrating" and "phasic" theories of $[Ca^{2+}]_{mito}$ changes during Ca transients were summarized by Dedkova and Blatter [8]. Among recent studies, rapid switches in $[Ca^{2+}]_i$ simulating Ca^{2+} transients in permeabilized cat ventricular myocytes by Sedova et al. [12] supports a "slow integrating" model, whereas in guinea-pig cardiomyocytes Maack et al. [23] observed rapid mitochondrial Ca^{2+} transients during every cytosolic Ca^{2+} transient elicited by voltage clamp pulses to initiate SR Ca^{2+} release. While these were both uncalibrated $[Ca^{2+}]_{mito}$ measurements they indicate extremes. Sometimes phasic $[Ca^{2+}]_{mito}$ transients have not been detected [12,31,32]. This could be either because the very small $[Ca^{2+}]_{mito}$ transients were simply below the detection limit, or because local SR Ca release events were not used (and may be essential as above). There may also be species differences in resting $[Na^+]_i$ or mitochondrial Ca^{2+} transport, such that beat-to-beat changes in $[Ca^{2+}]_{mito}$ have been seen in guinea-pig [41,42], but not in rat [22,43] and hamster [44,45]. The apparently large $[Ca^{2+}]_{mito}$ transients observed by Maack *et al.* [23] in guinea-pig myocytes (which seem to even limit $[Ca^{2+}]_i$ transients) are convincing, but seem to require PKA activation and strong cellular Ca^{2+} loading. We were unable to demonstrate substantially larger $[Ca^{2+}]_{mito}$ transients here by including cAMP to activate PKA (not shown).

Our work suggests that both phasic and integrative changes in $[Ca^{2+}]_{mito}$ occur, and we have added some quantitative framework to better understand the amplitude and kinetics of these components of $[Ca^{2+}]_{mito}$ control.

Supplementary Material

Refer to Web version on PubMed Central for supplementary material.

Acknowledgements

This work was supported by National Institute of Health Grants (R37-HL30077, P01-HL80101).

Abbreviations

SR
: Sarcoplasmic reticulum

$[Ca^{2+}]_{mito}$
: Intra-mitochondrial free Ca^{2+} concentration

$[Ca^{2+}]_i$
: Cytosolic Ca^{2+} concentration

mCU
: Mitochondrial Ca^{2+} uniporter

RaM
: Rapide mode of Ca^{2+} uptake

NCX_m
: Mitochondrial Na^+/Ca^{2+}-exchanger

$[Na^+]_i$
: Cytosolic Na^+ concentration

EC
: Excitation-contraction

RT
: room temperature

F_c
: Ca^{2+}-insensitive, isosbestic signal

References

1. Denton RM, McCormack JG. Ca^{2+} as a second messenger within mitochondria of the heart and other tissues. Annu Rev Physiol 1990;52:451–66. [PubMed: 2184763]
2. Bers DM. Calcium cycling and signaling in cardiac myocytes. Annu Rev Physiol 2008;70:23–49. [PubMed: 17988210]
3. Gunter TE, Pfeiffer DR. Mechanisms by which mitochondria transport calcium. Am J Physiol 1990 May;258(5 Pt 1):C755–86. [PubMed: 2185657]
4. Kirichok Y, Krapivinsky G, Clapham DE. The mitochondrial calcium uniporter is a highly selective ion channel. Nature 2004 Jan 22;427(6972):360–4. [PubMed: 14737170]
5. Buntinas L, Gunter KK, Sparagna GC, Gunter TE. The rapid mode of calcium uptake into heart mitochondria (RaM): comparison to RaM in liver mitochondria. Biochim Biophys Acta 2001 Apr 2;1504(2–3):248–61. [PubMed: 11245789]
6. Beutner G, Sharma VK, Lin L, Ryu SY, Dirksen RT, Sheu SS. Type 1 ryanodine receptor in cardiac mitochondria: transducer of excitation-metabolism coupling. Biochim Biophys Acta 2005 Nov 10;1717(1):1–10. [PubMed: 16246297]
7. Szalai G, Csordas G, Hantash BM, Thomas AP, Hajnoczky G. Calcium signal transmission between ryanodine receptors and mitochondria. J Biol Chem 2000 May 19;275(20):15305–13. [PubMed: 10809765]
8. Dedkova EN, Blatter LA. Mitochondrial Ca^{2+} and the heart. Cell Calcium 2008 Jul;44(1):77–91. [PubMed: 18178248]
9. Murphy E, Perlman M, London RE, Steenbergen C. Amiloride delays the ischemia-induced rise in cytosolic free calcium. Circ Res 1991 May;68(5):1250–8. [PubMed: 1902148]
10. Pogwizd SM, Sipido KR, Verdonck F, Bers DM. Intracellular Na in animal models of hypertrophy and heart failure: contractile function and arrhythmogenesis. Cardiovasc Res 2003 Mar 15;57(4): 887–96. [PubMed: 12650867]
11. Rizzuto R, Bernardi P, Favaron M, Azzone GF. Pathways for Ca^{2+} efflux in heart and liver mitochondria. Biochem J 1987 Sep 1;246(2):271–7. [PubMed: 3689311]
12. Sedova M, Dedkova EN, Blatter LA. Integration of rapid cytosolic Ca^{2+} signals by mitochondria in cat ventricular myocytes. Am J Physiol Cell Physiol 2006 Nov;291(5):C840–50. [PubMed: 16723510]
13. Bassani JW, Bassani RA, Bers DM. Relaxation in rabbit and rat cardiac cells: species-dependent differences in cellular mechanisms. J Physiol 1994 Apr 15;476(2):279–93. [PubMed: 8046643]
14. Maack C, O'Rourke B. Excitation-contraction coupling and mitochondrial energetics. Basic Res Cardiol 2007 Sep;102(5):369–92. [PubMed: 17657400]

15. Huser J, Blatter LA, Sheu SS. Mitochondrial calcium in heart cells: beat-to-beat oscillations or slow integration of cytosolic transients? J Bioenerg Biomembr 2000 Feb;32(1):27–33. [PubMed: 11768759]
16. Zhou Z, Neher E. Mobile and immobile calcium buffers in bovine adrenal chromaffin cells. J Physiol 1993 Sep;469:245–73. [PubMed: 8271200]
17. Uto A, Arai H, Ogawa Y. Reassessment of Fura-2 and the ratio method for determination of intracellular Ca^{2+} concentrations. Cell Calcium 1991 Jan;12(1):29–37. [PubMed: 2015620]
18. Pacher P, Csordas G, Hajnoczky G. Mitochondrial ca($^{2+}$) signaling and cardiac apoptosis. Biol Signals Recept 2001 May-Aug;10(3–4):200–23. [PubMed: 11351129]
19. Gunter TE, Gunter KK, Sheu SS, Gavin CE. Mitochondrial calcium transport: physiological and pathological relevance. Am J Physiol 1994 Aug;267(2 Pt 1):C313–39. [PubMed: 8074170]
20. Gunter TE, Buntinas L, Sparagna G, Eliseev R, Gunter K. Mitochondrial calcium transport: mechanisms and functions. Cell Calcium 2000 Nov-Dec;28(5–6):285–96. [PubMed: 11115368]
21. Seguchi H, Ritter M, Shizukuishi M, Ishida H, Chokoh G, Nakazawa H, et al. Propagation of Ca^{2+} release in cardiac myocytes: role of mitochondria. Cell Calcium 2005 Jul;38(1):1–9. [PubMed: 15993240]
22. Griffiths EJ. Species dependence of mitochondrial calcium transients during excitation-contraction coupling in isolated cardiomyocytes. Biochem Biophys Res Commun 1999 Sep 24;263(2):554–9. [PubMed: 10491330]
23. Maack C, Cortassa S, Aon MA, Ganesan AN, Liu T, O'Rourke B. Elevated cytosolic Na^{+} decreases mitochondrial Ca^{2+} uptake during excitation-contraction coupling and impairs energetic adaptation in cardiac myocytes. Circ Res 2006 Jul 21;99(2):172–82. [PubMed: 16778127]
24. Bell CJ, Bright NA, Rutter GA, Griffiths EJ. ATP regulation in adult rat cardiomyocytes: time-resolved decoding of rapid mitochondrial calcium spiking imaged with targeted photoproteins. J Biol Chem 2006 Sep 22;281(38):28058–67. [PubMed: 16882672]
25. Trollinger DR, Cascio WE, Lemasters JJ. Selective loading of Rhod 2 into mitochondria shows mitochondrial Ca^{2+} transients during the contractile cycle in adult rabbit cardiac myocytes. Biochem Biophys Res Commun 1997 Jul 30;236(3):738–42. [PubMed: 9245725]
26. O'Neill SC, Miller L, Hinch R, Eisner DA. Interplay between SERCA and sarcolemmal Ca^{2+} efflux pathways controls spontaneous release of Ca^{2+} from the sarcoplasmic reticulum in rat ventricular myocytes. J Physiol 2004 Aug 15;559(Pt 1):121–8. [PubMed: 15194743]
27. Terentyev D, Kubalova Z, Valle G, Nori A, Vedamoorthyrao S, Terentyeva R, et al. Modulation of SR Ca release by luminal Ca and calsequestrin in cardiac myocytes: effects of CASQ2 mutations linked to sudden cardiac death. Biophys J 2008 Aug;95(4):2037–48. [PubMed: 18469084]
28. MacQuaide N, Dempster J, Smith GL. Measurement and modeling of Ca^{2+} waves in isolated rabbit ventricular cardiomyocytes. Biophys J 2007 Oct 1;93(7):2581–95. [PubMed: 17545234]
29. Macquaide N, Smith GL. 487.11-Pos Quantification Of SR Depletion During Spontaneous Ca^{2+} Waves In Ventricular Cardiomyocytes. Biophys J 2008 February 1;94(1MeetingAbstracts):487–k.
30. Gavin CE, Gunter KK, Gunter TE. Mn^{2+} sequestration by mitochondria and inhibition of oxidative phosphorylation. Toxicol Appl Pharmacol 1992 Jul;115(1):1–5. [PubMed: 1631887]
31. Miyata H, Silverman HS, Sollott SJ, Lakatta EG, Stern MD, Hansford RG. Measurement of mitochondrial free Ca^{2+} concentration in living single rat cardiac myocytes. Am J Physiol 1991 Oct; 261(4 Pt 2):H1123–34. [PubMed: 1928394]
32. Zhou Z, Matlib MA, Bers DM. Cytosolic and mitochondrial Ca^{2+} signals in patch clamped mammalian ventricular myocytes. J Physiol 1998 Mar 1;507(Pt 2):379–403. [PubMed: 9518700]
33. Liu T, O'Rourke B. Enhancing mitochondrial Ca^{2+} uptake in myocytes from failing hearts restores energy supply and demand matching. Circ Res 2008 Aug 1;103(3):279–88. [PubMed: 18599868]
34. Bassani RA, Bassani JW, Bers DM. Mitochondrial and sarcolemmal Ca^{2+} transport reduce $[Ca^{2+}]i$ during caffeine contractures in rabbit cardiac myocytes. J Physiol 1992;453:591–608. [PubMed: 1464847]
35. Csordas G, Thomas AP, Hajnoczky G. Calcium signal transmission between ryanodine receptors and mitochondria in cardiac muscle. Trends Cardiovasc Med 2001 Oct;11(7):269–75. [PubMed: 11709280]

36. Sharma VK, Ramesh V, Franzini-Armstrong C, Sheu SS. Transport of Ca^{2+} from sarcoplasmic reticulum to mitochondria in rat ventricular myocytes. J Bioenerg Biomembr 2000 Feb;32(1):97–104. [PubMed: 11768767]
37. Garcia-Perez C, Hajnoczky G, Csordas G. Physical Coupling Supports the Local Ca^{2+} Transfer between Sarcoplasmic Reticulum Subdomains and the Mitochondria in Heart Muscle. J Biol Chem 2008 Nov 21;283(47):32771–80. [PubMed: 18790739]
38. Ramesh V, Sharma VK, Sheu SS, Franzini-Armstrong C. Structural proximity of mitochondria to calcium release units in rat ventricular myocardium may suggest a role in Ca^{2+} sequestration. Ann N Y Acad Sci 1998 Sep 16;853:341–4. [PubMed: 10603975]
39. Pacher P, Thomas AP, Hajnoczky G. Ca^{2+} marks: miniature calcium signals in single mitochondria driven by ryanodine receptors. Proc Natl Acad Sci U S A 2002 Feb 19;99(4):2380–5. [PubMed: 11854531]
40. McCormack JG, Browne HM, Dawes NJ. Studies on mitochondrial Ca^{2+}-transport and matrix Ca^{2+} using fura-2-loaded rat heart mitochondria. Biochim Biophys Acta 1989 Mar 23;973(3):420–7. [PubMed: 2923871]
41. Isenberg G, Han S, Schiefer A, Wendt-Gallitelli MF. Changes in mitochondrial calcium concentration during the cardiac contraction cycle. Cardiovasc Res 1993 Oct;27(10):1800–9. [PubMed: 8275527]
42. Griffiths EJ, Stern MD, Silverman HS. Measurement of mitochondrial calcium in single living cardiomyocytes by selective removal of cytosolic indo 1. Am J Physiol 1997 Jul;273(1 Pt 1):C37–44. [PubMed: 9252440]
43. Horikawa Y, Goel A, Somlyo AP, Somlyo AV. Mitochondrial calcium in relaxed and tetanized myocardium. Biophys J 1998 Mar;74(3):1579–90. [PubMed: 9512053]
44. Moravec CS, Desnoyer RW, Milovanovic M, Schluchter MD, Bond M. Mitochondrial calcium content in isolated perfused heart: effects of inotropic stimulation. Am J Physiol 1997 Sep;273(3 Pt 2):H1432–9. [PubMed: 9321835]
45. Moravec CS, Bond M. Effect of inotropic stimulation on mitochondrial calcium in cardiac muscle. J Biol Chem 1992 Mar 15;267(8):5310–6. [PubMed: 1544913]

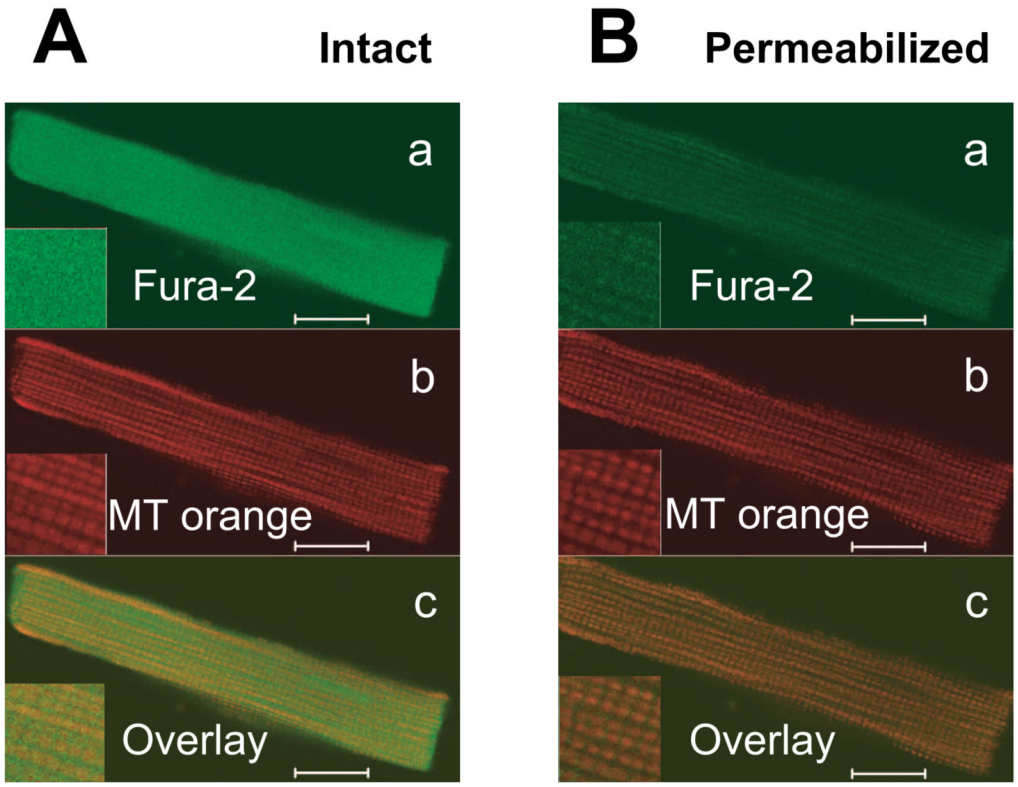

Figure 1. Mitochondrial localization of fura-2 in permeabilized myocytes

Confocal images of intact rat ventricular cardiomyocyte simultaneously loaded with fura-2 and Mitotracker Orange before (A) and after sarcolemmal permeabilization by saponin (B). Top panels (a) are fura-2 signals, middle panels (b) are Mitotracker Orange, showing typical mitochondrial pattern and lower panels (c) show merged images. Fura-2 only colocalizes with mitochondria after permeabilization. Scale bars are equal 10 μm.

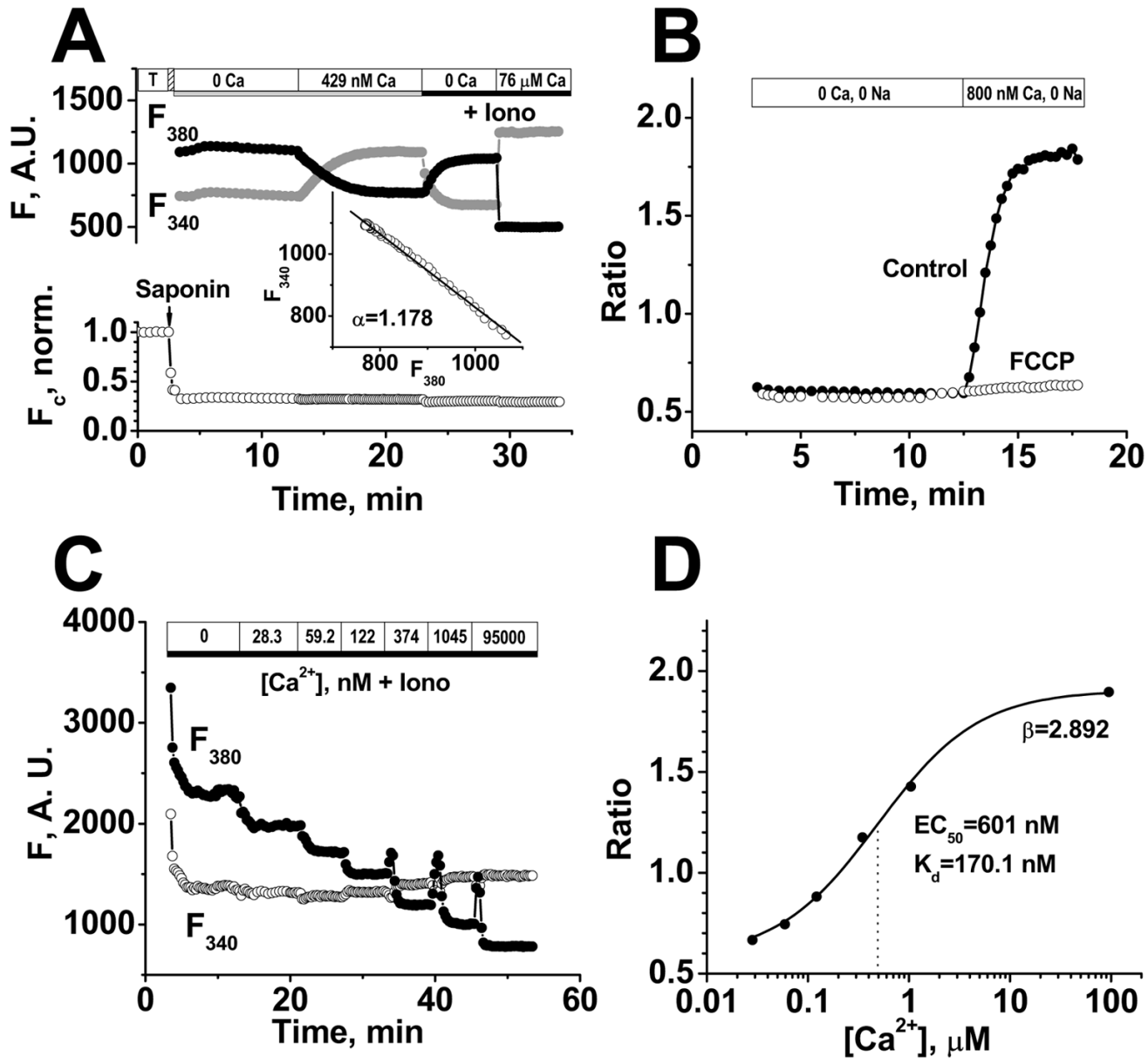

FIGURE 2. Mitochondrial free [Ca^{2+}] measurements with fura-2

A, Top traces show background-corrected fura-2 fluorescence at 340 and 380 nm excitation after permeabilization. The inset shows plot of F_{340} vs. F_{380} as $[Ca^{2+}]_{mito}$ varies to determine αand allows measurement of F_c (Ca^{2+}-independent fura-2 fluorescence) in bottom normalized trace showing loss of 70% of fura-2 upon permeabilization. B, Rise in $[Ca^{2+}]_{mito}$ in the presence of 800 nM Ca^{2+} and in the absence of Na^+ (±2.5 μM FCCP added 2 min prior to increasing $[Ca^{2+}]_i$). C, *In situ* calibration of background subtracted fura-2 fluorescence in permeabilized cells in the presence of 3 μM ionomycin (Iono), 10 μM FCCP and 20 μg/mL oligomycin. D, Fura-2 ratio dependence on $[Ca^{2+}]_i$ for data in C fit to $[Ca^{2+}] = K_d\beta(R\text{-}R_{min})/(R_{max}\text{-}R)$, where $EC_{50} = K_d\beta$ and $\beta = F_{380\text{-}max}/F_{380\text{-}min}$.

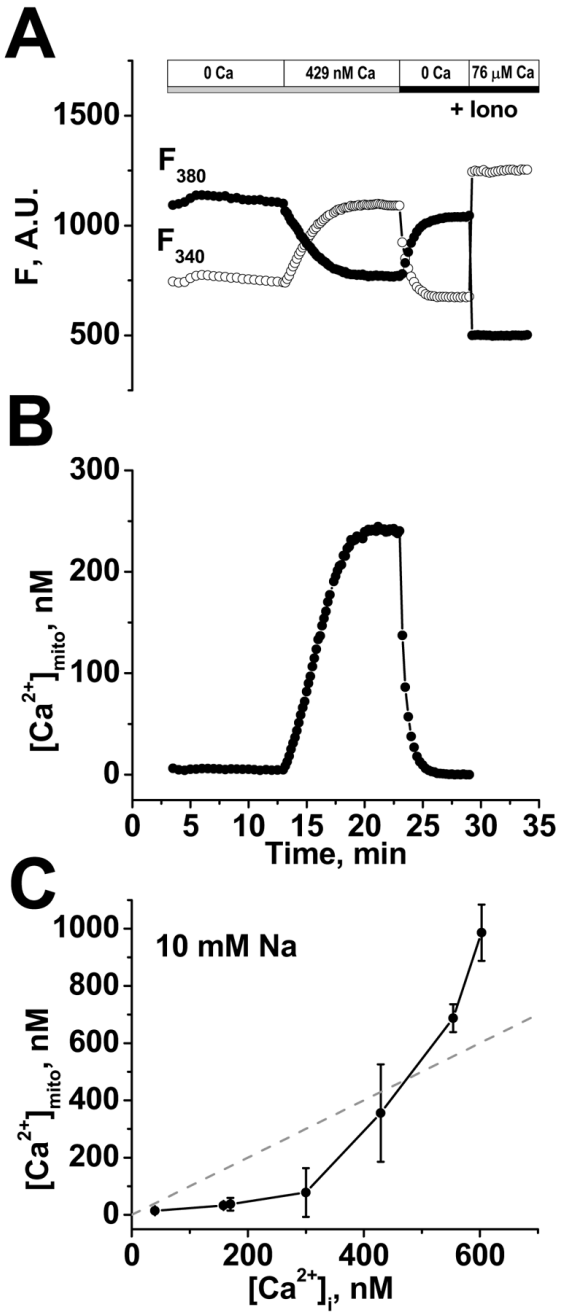

FIGURE 3. Steady-state dependence of $[Ca^{2+}]_{mito}$ on $[Ca^{2+}]_i$

A, example of background-corrected raw F_{340} and F_{380} 380 nm signals, where $[Ca^{2+}]_i$ was raised from 0 to 429 nM, with R_{min} and R_{max} measured at the end using ionophores (Iono). B, calibrated $[Ca^{2+}]_{mito}$ calculated from A. C, Steady-state dependence of $[Ca^{2+}]_{mito}$ on $[Ca^{2+}]_i$ in the presence of 10 mM Na^+ (Mean ±SD, n=3–7 myocytes).

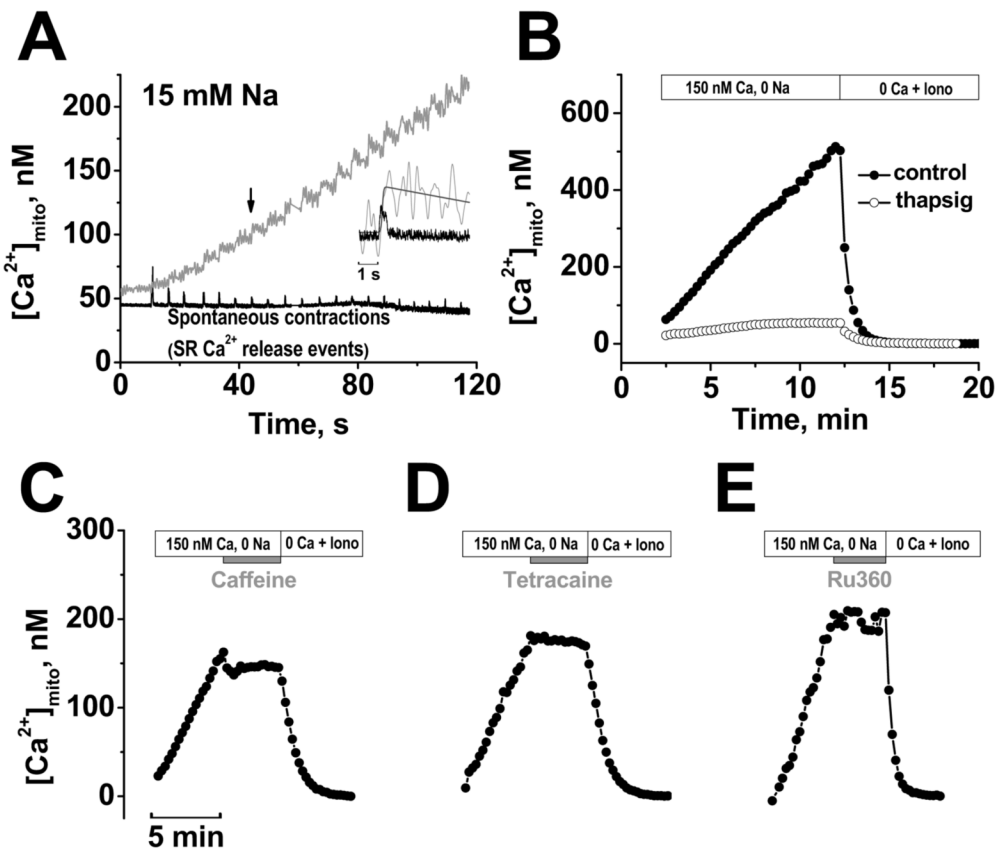

FIGURE 4. $[Ca^{2+}]_{mito}$ during cyclical SR Ca^{2+} release

A, Simultaneous recording of $[Ca^{2+}]_{mito}$ (grey) and contractions (black) in the presence of 150 nM Ca^{2+} and 15 mM Na^{+}. 40 μM cytochalasin D was included to limit contraction. Inset shows expanded superimposed traces for the 7th contraction (traces smoothed by fast Fourier transform). B, $[Ca^{2+}]_{mito}$ under control conditions and after pretreated with 1 μM thapsigargin for 30 min. Mitochondrial Ca^{2+} uptake was halted by acute application of 10 mM caffeine (C), 2 mM tetracaine (D), or 1 μM Ru360 (E). Each experiment ended with Ca^{2+}-free solution with ionophores (Iono) to start calibration.

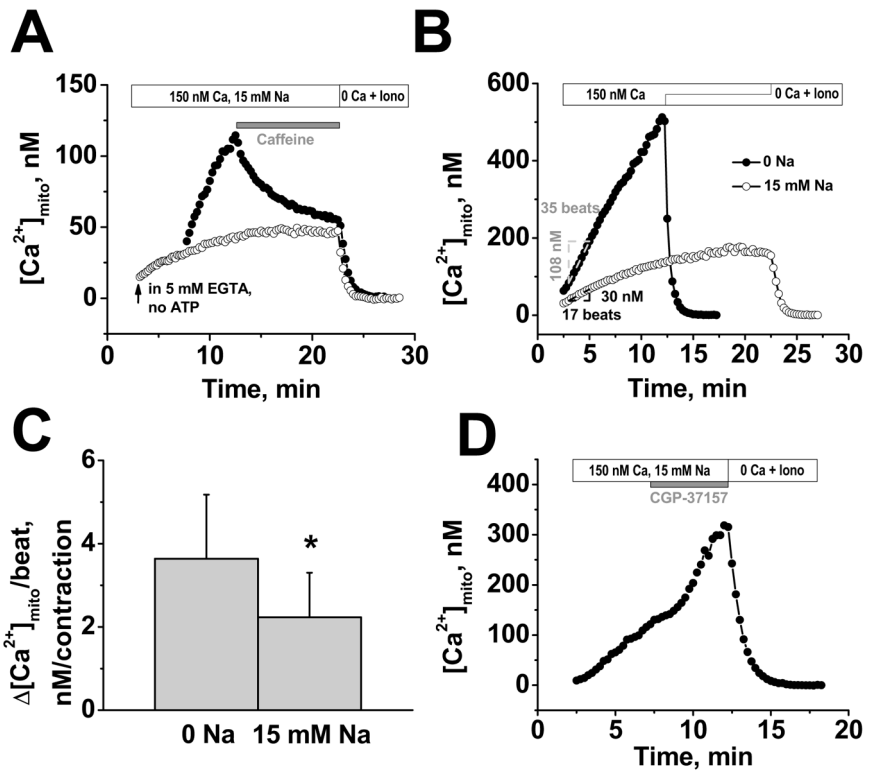

FIGURE 5. Calibrated rise in $[Ca^{2+}]_{mito}$ per beat and $[Na^{+}]_i$-dependence

A, 10 mM caffeine stops $[Ca^{2+}]_{mito}$, but with 15 mM Na^+ $[Ca^{2+}]_{mito}$ declines (filled symbols); mitochondrial Ca^{2+} uptake in presence of 5 mM EGTA (empty symbols). B, examples of $[Ca^{2+}]_{mito}$ increase per contraction (±15 mM Na^+). C, Average increase of $[Ca^{2+}]_{mito}$ per contraction (±15 mM Na^+). D, Blockade of NCX_m (5 μM CGP-37157) increases rate of $[Ca^{2+}]_{mito}$ rise in presence of 15 mM Na^+. Each experiment ended with Ca^{2+}-free solution with ionophores (Iono) to start calibration.

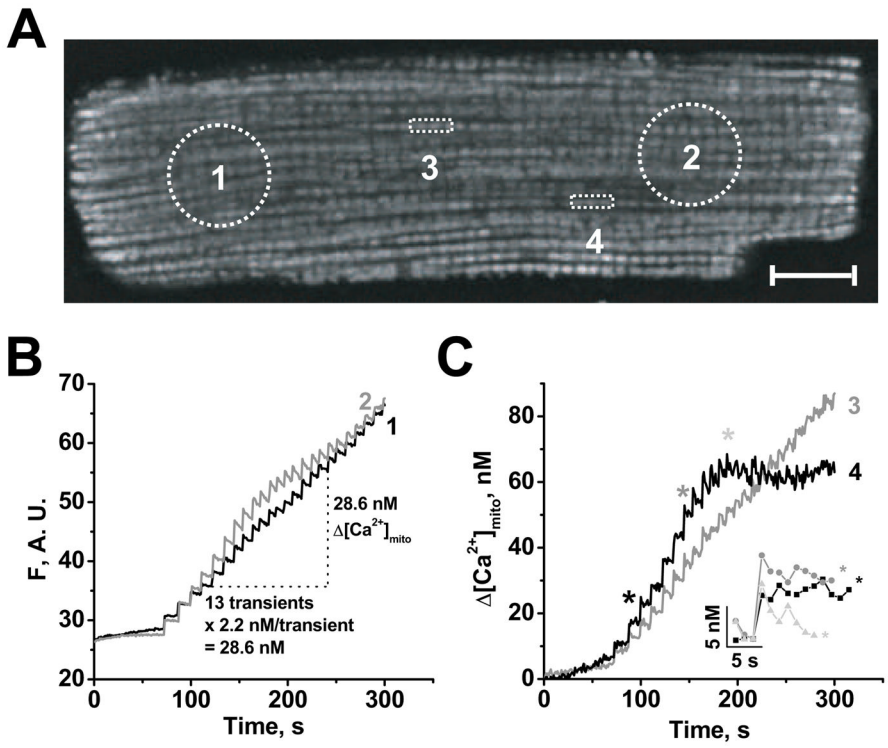

FIGURE 6. Spatially resolved $[Ca^{2+}]_{mito}$ during SR Ca^{2+} release

A, confocal image of permeabilized rat ventricular myocyte loaded with 10 μM rhod-2 AM, after 5 min of spontaneous Ca^{2+} transients in 15 mM Na^{+} (with 80 μM cytochalasin D) with 4 regions of interest (ROI) indicated. Scale bar is equal 10 μm. B-C, Time courses of $[Ca^{2+}]_{mito}$ in 4 ROIs, either as fluorescence (F in arbitrary units, B) or calibrated $\Delta[Ca^{2+}]_{mit}$ (C) using averaged $\Delta[Ca^{2+}]_{mito}$/beat from Fig. 5C (see B and text). C, ROI 3 and 4 contain 3 mitochondria and inset shows the indicated $[Ca^{2+}]_{mito}$ transients expanded.

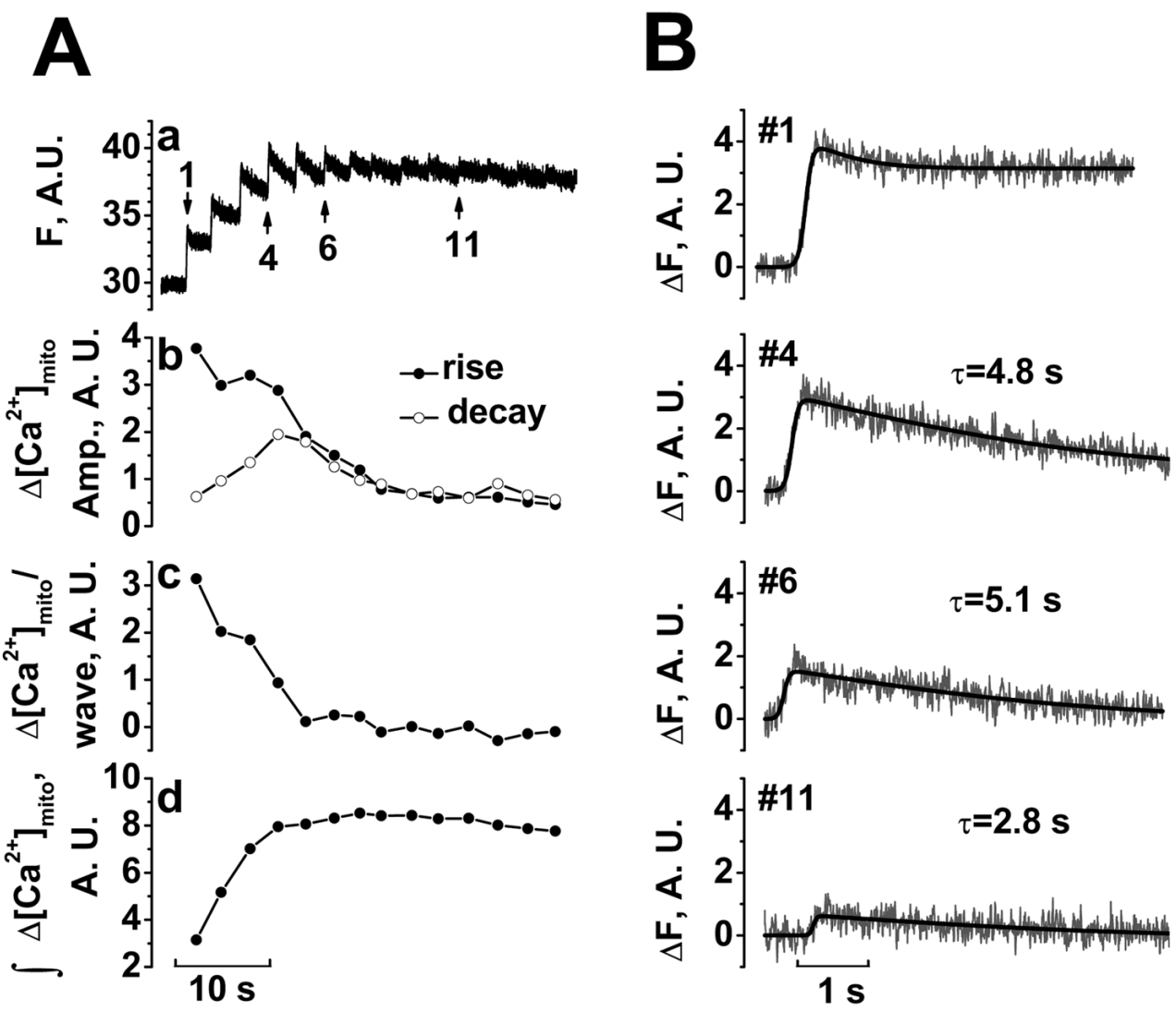

FIGURE 7. Mitochondrial [Ca^{2+}] balance during SR Ca^{2+} release

Aa, $[Ca^{2+}]_{mito}$ measured in line-scan images in permeabilized myocyte loaded with 5 μM rhod-2 AM in 15 mM Na^{+} (with 80 μM cytochalasin D; subjected to 5 point smoothing). Ab, Amplitudes of rise (filled symbols) and decay phase (empty symbols). Ac, Net gain in $[Ca^{2+}]_{mito}$ per wave. Ad, Integral of change in $[Ca^{2+}]_{mito}$. B, Expanded and curve fitting for the transients indicated in A.

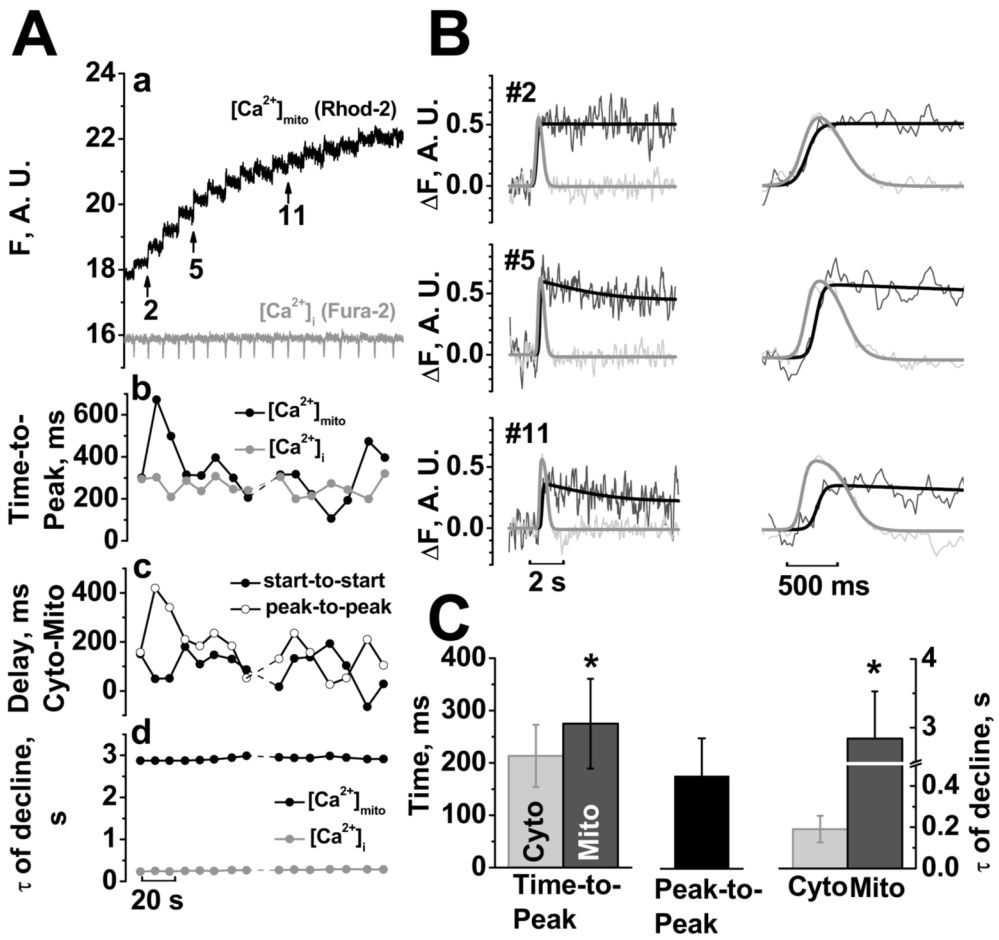

FIGURE 8. Kinetics of $[Ca^{2+}]_{mito}$ vs. $[Ca^{2+}]_i$ signals

Aa, $[Ca^{2+}]_{mito}$ and $[Ca^{2+}]_i$ measured in line-scan images in permeabilized myocyte with mitochondrial rhod-2 and 5 μM cytosolic fura-2 salt (15 mM Na^+, 80 μM cytochalasin D, 5 point smoothing). Ab, Time-to-Peak (rise time for either $[Ca^{2+}]_{mito}$ or $[Ca^{2+}]_i$). Ac, Delay of $[Ca^{2+}]_{mito}$ after $[Ca^{2+}]_i$ as start-to-start and peak-to-peak, Ad, time constant τof decline. B, Curve fitting and expanded mitochondrial (black) and cytosolic (grey) transients indicated in Aa. C, Difference in mitochondrial and cytosolic kinetics (n=3 cells, 25 transients).